# Spatial Characterization of Flood Magnitudes over the Drainage Network of the Delaware River Basin

PING LU, JAMES A. SMITH, AND NING LIN

*Department of Civil and Environmental Engineering, Princeton University, Princeton, New Jersey*

(Manuscript received 17 March 2016, in final form 23 December 2016)

ABSTRACT

A framework to characterize the distribution of flood magnitudes over large river networks is developed using the Delaware River basin in the northeastern United States as a principal study region. Flood magnitudes are characterized by the flood index, which is defined as the ratio of the flood peak for a flood event to the historical 10-yr flood magnitude. Event flood peaks are computed continuously over the drainage network using a distributed hydrologic model, CUENCAS, with high-resolution radar rainfall fields as the principal forcing. The historical 10-yr flood is calculated based on scaling relationships between the 10-yr flood and drainage area. Summary statistics for characterizing the probability distribution and spatial correlation of flood magnitudes over the drainage network are developed based on the flood index. This framework is applied to four flood events in the Delaware River basin that reflect the principal flood-generating mechanisms in the eastern United States: landfalling tropical cyclones (Hurricane Ivan in September 2004 and Hurricane Irene in August 2011), late winter/early spring extratropical systems (April 2005), and warm season convective systems (June 2006). The framework can be utilized to characterize the spatial distribution of floods, most notably for floods caused by landfalling tropical cyclones, which play an important role in controlling the upper tail of flood peak magnitudes over much of the eastern United States.

## 1. Introduction

One of the most challenging aspects of flood hazard characterization is assessing the spatial extent of flooding. The spatial distribution of flood magnitudes reflects the interplay of rainfall variability in time and space with land surface properties that influence infiltration and runoff production, and with the network structure of the channel system (Blöschl et al. 2007, 2013; Sivapalan et al. 1987; Sivapalan 2003; Laaha et al. 2012; Ayalew et al. 2014a,b; Javier et al. 2010; Merz et al. 2008). Rainfall structure and evolution can vary substantially from storm to storm, resulting in striking contrasts in the spatial distribution of flood magnitudes over the drainage network.

Villarini and Smith (2010) introduced the flood index as the ratio of flood peak discharge at a particular location along a river network to the 10-yr flood discharge at the same location, as a dimensionless representation of flood magnitudes that could be used to examine the spatial distribution of flooding over large regions. Their analyses were based on observations from a network of U.S. Geological Survey (USGS) stream gauging stations. The spatial distribution of flooding was represented by a continuous spatial field of flood index values obtained by inverse-distance-weighted interpolation of discrete point observations. The flood index has been shown to be highly correlated with flood damage for tropical cyclone flooding (Czajkowski et al. 2013, 2017). A disadvantage of this method is that the spatial structure of the river network is not directly taken into consideration.

In this study, we develop tools for examining spatial structure of flooding through integration of the spatial and temporal information from high-resolution observations of rainfall fields into a spatially distributed hydrologic model. We adopt a physics-based representation for runoff generation and routing in the river network, with a particular focus on the interplay of rainfall variability in time and space with network structure of the watershed. The hydrological model CUENCAS (Mantilla and Gupta 2005; Cunha 2012) is chosen based on its successful application for flood characterization in large drainage basins. Its hillslope–link basin decomposition provides an efficient and accurate representation of the river network. In CUENCAS, model formulations are designed to reduce the need for calibration, and parameterization is based on readily available datasets,

*Corresponding author e-mail*: Ping Lu, pingl@princeton.edu

DOI: 10.1175/JHM-D-16-0071.1

enabling the model to give realistic simulation of floods continuously over a river network.

We use the flood index, here defined as the ratio of the simulated event flood peak and the historical 10-yr flood magnitude, to represent the flood magnitudes continuously over the drainage network. To summarize the flood characteristics and compare them across events, we develop a statistical framework to characterize the probability distribution of flood index values over the drainage network. These probability distributions are examined for the entire basin and are used to characterize the spatial variation of flood magnitudes for flood events. We examine the scale-dependent distribution of flood magnitudes using multiple representations of the basin scale, including drainage area, stream length, and the Horton stream order. We also develop metrics to characterize the correlation structure of flood index over the network, especially along the main stem. Other approaches for analysis of flood magnitude continuously over the drainage network include those based on topological kriging (see Skøien et al. 2005; Merz et al. 2008).

Regulation by dams affects flood response in portions of the Delaware River basin, as in most major river basins of the United States and around the world. Detailed information on dam operations, however, is rarely available, especially during flood periods. Furthermore, discharge observations from dams are not routinely available. We use a simple low-pass-filter representation of dam impacts on downstream flooding in our CUENCAS model implementation. For the Delaware River basin, this formulation is consistent with previous analyses of the downstream impacts of dams on flood response (Smith et al. 2010). We will show that it also provides an improved representation of flood response for the four flood events that we analyze. This approach is not suited for all applications, especially those that directly address the impacts of operations of specific dams on flood response. It does, however, provide useful insight into the impacts of dams on the spatial extent of flooding over a river network.

We apply the modeling and analysis framework to four storms, which resulted in the largest floods in Delaware River basin (in terms of flood peaks at the basin outlet) since the flood of 1955 caused by Hurricanes Connie and Diane. The four floods reflect the principal flood-generating mechanisms in the eastern United States (Smith et al. 2010): landfalling tropical cyclones (Hurricane Ivan in September 2004 and Hurricane Irene in August 2011), late winter/early spring extratropical systems (April 2005), and warm season convective systems (June 2006). The hydrology and hydrometeorology of the 2004, 2005, and 2006 floods have been summarized in Smith et al. (2010).

Tropical cyclones represent a particularly important flood hazard for the eastern United States, especially in controlling the upper tail of flood peak distributions (Villarini and Smith 2010). The framework that we develop for examining the spatial distribution of flood magnitudes over a drainage network will be used for examining the distribution of tropical cyclone flood peaks, in both the current and future climates. We will use large samples of tropical cyclone storm sets (Emanuel et al. 2006, 2008; Zhu et al. 2013) to assess flood hazards over the eastern United States.

The paper is organized as follows. In section 2, we describe the hydrological model CUENCAS and introduce the flood index and statistical framework for examining flood magnitudes over the drainage network. In section 3, we describe the study area and the four storm events. In section 4, we present hydrological modeling results, flood index statistics, and rainfall field analysis. In section 5, we summarize major findings.

## 2. Methodology

### a. Hydrologic modeling

In this study we apply a hillslope-based hydrological model, CUENCAS, which has been applied in a wide range of flood hydrology applications (Mantilla and Gupta 2005; Cunha 2012). In CUENCAS, the drainage basin is treated as a collection of hillslopes connected by channel links, which are compartmentalized and derived from a high-resolution digital elevation model (DEM). The river network is represented as a binary tree defined by links and nodes. From the DEM, we extract information about the position and geometry of each link, and the way links are connected. CUENCAS provides a flexible representation of hydrologic modeling components. At the hillslope scale, infiltration is calculated based on the Soil Conservation Service Curve Number (SCS-CN) method (NRCS 1986; Mishra and Singh 1999). The advantages of the SCS-CN approach are its parsimonious parameterization and broad application (Ponce and Hawkins 1996). In CUENCAS, the SCS-CN method is enhanced for continuous hydrologic simulation, taking into account the temporal and spatial variability of the curve number (Michel et al. 2005; Durbude et al. 2011; Cunha 2012).

Flow velocity from hillslope to the channel network is computed using Manning's equation (Cunha et al. 2012; Cunha 2012). Along the river network, flow is routed using a power-law representation of the channel velocity $v$ in terms of discharge and upstream area (Mantilla 2007):

$$v = v_0 \times q^{\lambda_1} \times A^{\lambda_2}, \tag{1}$$

where $q$ is the instantaneous discharge for the link (also the outflow from the link), $A$ is upstream drainage area,

$v_0$ is the reference channel velocity, and $\lambda_1$ and $\lambda_2$ are parameters based on hydraulic geometry studies (Mantilla 2007; Paik and Kumar 2004).

The Delaware River basin is decomposed into 1891 hillslopes and 1891 links. The area of hillslopes varies from less than 0.1 to 78 km$^2$. The length of links varies from less than 0.1 to 22 km. The model runs in a storm event mode, with the initial soil moisture taken from monthly mean CPC soil moisture data and hourly rainfall taken from NCEP stage IV at 4-km spatial resolution. Model parameters (i.e., $v_0$, $\lambda_1$, and $\lambda_2$) are computed following Mantilla (2007) and Paik and Kumar (2004).

### b. Flood index

Flood peak magnitudes are transformed into the dimensionless flood index $Z$, which is formulated as

$$Z = \frac{Q_p}{Q_{10}}, \tag{2}$$

where $Q_p$ is the peak discharge during the event at a specific location and $Q_{10}$ is the 10-yr flood at the same location. In this study, $Q_p$ is estimated using CUENCAS with observed radar rainfall fields as the principal forcing, and the corresponding 10-yr flood is estimated based on historical flood records from USGS stream gauging stations. The 10-yr flood is estimated using a power-law scaling representation of flood quantiles developed from observed annual flood peak observations in the drainage basin. We assume that $T$ (yr) flood quantiles $Q_T$ and drainage area $A$ have a power-law relationship (Villarini and Smith 2010):

$$Q_T = \alpha_T \left(\frac{A}{A_0}\right)^{\beta_T}. \tag{3}$$

The scaling parameters $\alpha_T$ and $\beta_T$ are computed by means of the Levenberg–Marquardt algorithm; the reference drainage area $A_0$ is taken to be 1000 km$^2$.

The 10-yr flood can be calculated in a variety of ways. The approach we take in this paper is designed to provide a simple implementation and illustration of the modeling framework. For specific applications, more detailed representations of the 10-yr flood may be developed. Flood quantiles in a region can vary with both drainage area and other physical properties of the drainage basin (Ayalew 2015), and multivariate statistical methods have been widely used to develop regional estimation equations for flood quantiles (Stedinger 1983; Stedinger and Tasker 1985, 1986). These approaches can utilize the information in covariates for which systematic datasets are available in the United States (Falcone 2011). In addition to the applications-oriented development of regional regression equations, this line of research provides important insights to dependence of flood magnitudes on drainage basin properties. In some settings the 10-yr flood can be estimated based on computed peak discharges from hydrologic modeling using long rainfall records (Moser et al. 2015). A challenge in implementing such a model-based approach is developing suitable rainfall datasets. The resampling methods introduced by Wright et al. (2014) provide a promising line of research for advancing this approach. Future research will examine the development of improved statistical and model-based methods for computing the 10-yr floods based on resampling methods.

### c. Statistics for spatial analysis of the flood index

Previous studies have analyzed the distributions and joint distributions of flood peaks, flood volumes, and flood durations based on samples of observations at stream gauging stations (Krstanovic and Singh 1987; Sackl and Bergmann 1987; Goel et al. 1998; Yue 1999; Villarini and Smith 2010). A disadvantage of analyses based solely on point observations is that the river network structure is not fully taken into consideration. In addition, the analysis is dependent on the specific locations of gauging stations and the number of available stations.

The drainage network can be represented as a tree graph that consists of a set of nodes connected to one another through links such that there are no loops in the graph. The outlet node imposes flow direction. For each node there is a unique path (i.e., sequence of nodes and links) to the outlet. A source is a node, other than the outlet, connected only to one link. A junction is a node connected to more than one link. Exterior links connect sources to junctions. Interior links connect two junctions. The number of links in the drainage network will be denoted by $n$, and an order is imposed on the stream links. The Horton stream order represents the relative size of a river segment. Links with Horton stream order 1 are stream segments with no tributaries, links with Horton stream order 2 are on streams formed by the confluence of first-order streams, and more generally, links downstream of the confluence of two links of order $i$ have order $i + 1$. Finally, links downstream of the confluence of two links of order $i$ and $i + j$, for $j$ greater than 0, take the higher order, $i + j$, of the two upstream links. We use the following notation to represent the drainage network and flood index over the drainage network:

$n$ = number of links in the drainage network;
$\omega_i$ = order of link $i$;
$l_i$ = channel length of link $i$;
$A_i$ = area above link $i$, including the local area;
$d_{ik}$ = flow distance from link $i$ to link $k$: positive for $k$ downstream of $i$, negative for $k$ upstream of $i$, and 0 for $i$ and $k$ on different flow paths to the outlet;

$\mathbf{e}_{ik}$ = vector with 1) flow distance from link $i$ to the confluence of the flow path with link $k$ and 2) flow distance from link $k$ to the confluence of the flow path of link $i$. For $i$ and $k$ in the same flow path both values are $-1$.

Given a sample of flood events, we denote the flood index for link $i$ of the $j$th flood event by $Z_{ij}$. One of the most important statistics summarizing the spatial structure of flooding over the drainage network is the fraction of the drainage network with flood index less than or equal to $z$,

$$I_j(z) = \frac{1}{\sum_{i=1}^{n} l_i} \sum_{i=1}^{n} l_i 1(Z_{ij} \le z), \tag{4}$$

where the indicator function $1(Z_{ij} \le z)$ takes the value 1 if $Z_{ij} \le z$ and 0 otherwise. Function $I_j(1)$ represents the fraction of the drainage network that has flood peak values less than the 10-yr flood; $I_j(2)$ represents the fraction of the drainage network with flood peak values less than twice the 10-yr flood. Function $I_j(z)$ is a monotonically nondecreasing function of $z$ and takes values between 0 and 1, implying that it has the form of a cumulative distribution function. This statistic provides the most basic tool for distinguishing flood magnitudes among a sample of flood events.

Some flood events in the Delaware River basin have a greater impact on higher-order stream channels than on lower-order stream channels (Smith et al. 2010). In general, we would like to develop tools for characterizing the contrasting flood magnitudes dependent on the scale. One statistic that we will use for this purpose is the fraction of $m$th-order channel links with flood index less than or equal to $z$:

$$I_j(z,m) = \frac{1}{\sum_{i=1}^{n} l_i 1(\omega_i = m)} \sum_{i=1}^{n} l_i 1(Z_{ij} \le z) 1(\omega_i = m). \tag{5}$$

We will see below that there are contrasting scale-dependent flood response properties among the four flood events and systematic dependencies of flood magnitude on stream order.

The mean flood index

$$\overline{Z}_j = \frac{1}{\sum_{i=1}^{n} l_i} \sum_{i=1}^{n} l_i Z_{ij} \tag{6}$$

provides a simple statistic for representing the central tendency of flood magnitudes. We will also condition the mean flood index on stream order,

$$\overline{Z}_j(m) = \frac{1}{\sum_{i=1}^{n} l_i 1(\omega_i = m)} \sum_{i=1}^{n} l_i Z_{ij} 1(\omega_i = m). \tag{7}$$

Flooding along the main stem of major rivers is an important element of flood hazards in many settings. Flood magnitudes on a drainage network are spatially correlated because of the inherent rainfall structure and by the nature of the hydrological processes that control flood response in the watershed. Here we use Pearson correlation coefficient $\rho_j(d)$ to measure the strength of linkage of upstream and downstream flood index separated by distance $d$ over the main stem (with $s$ links):

$$\rho_j(d) = \frac{\sum_{i=1}^{s}\sum_{k=1}^{s} (Z_{ij} - \hat{Z}_{ij})(Z_{kj} - \hat{Z}_{kj}) 1(d_{ik} = d)}{\sqrt{\sum_{i=1}^{s}\sum_{k=1}^{s} (Z_{ij} - \hat{Z}_{ij})^2 1(d_{ik} = d)} \sqrt{\sum_{i=1}^{s}\sum_{k=1}^{s} (Z_{kj} - \hat{Z}_{kj})^2 1(d_{ik} = d)}}, \quad \text{where}$$

$$\hat{Z}_{ij} = \frac{\sum_{i=1}^{s}\sum_{k=1}^{s} Z_{ij} 1(d_{ik} = d)}{\sum_{i=1}^{s}\sum_{k=1}^{s} 1(d_{ik} = d)} \quad \text{and}$$

$$\hat{Z}_{kj} = \frac{\sum_{i=1}^{s}\sum_{k=1}^{s} Z_{kj} 1(d_{ik} = d)}{\sum_{i=1}^{s}\sum_{k=1}^{s} 1(d_{ik} = d)}. \tag{8}$$

We will principally use this statistic to examine contrasting properties of flood index along the main channel of the river reach among different flood events.

Stream junctions introduce a unique element of variability in flood magnitudes. Flood magnitudes downstream reflect the rainfall and flood response

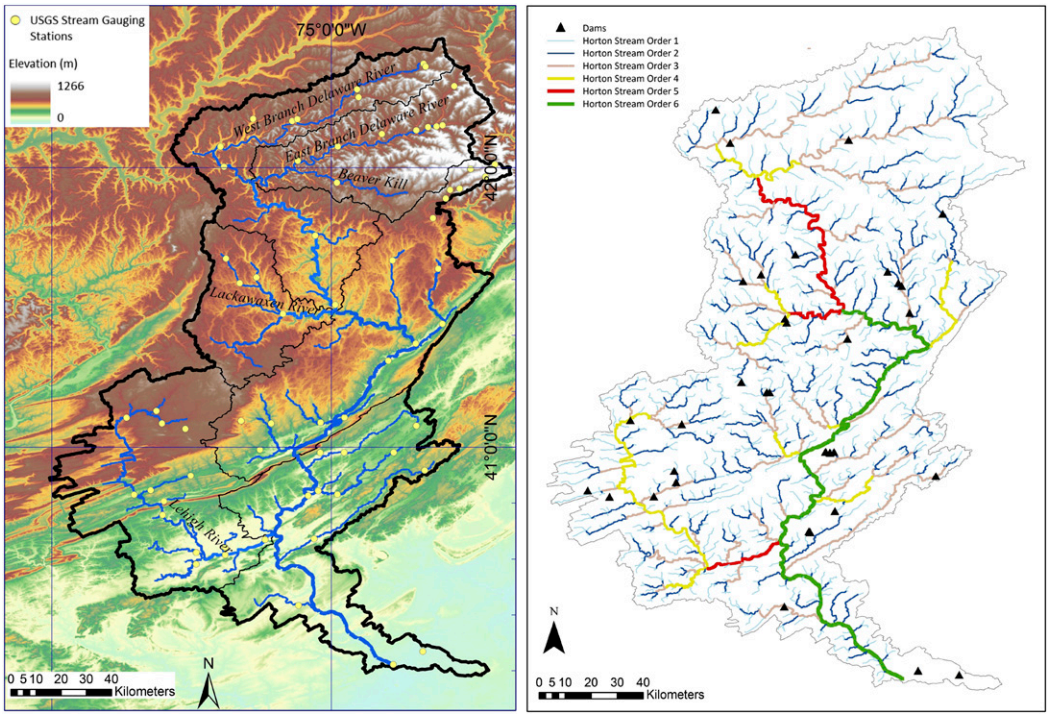


FIG. 1. Map of Delaware River basin showing (left) elevation and river network and (right) Horton stream order and location of dams.

from two disjoint regions. One statistic for characterizing correlation structure of flood magnitudes focusing on stream junctions is the confluence covariance $C_j$, which is given by

$$C_j = \frac{1}{\sum_{i=1}^{n}\sum_{k=1}^{n} 1(\mathbf{e}_{ik} = \mathbf{0})} \sum_{i=1}^{n}\sum_{k=1}^{n} (Z_{ij} - \hat{Z}_j)(Z_{kj} - \hat{Z}_j) 1(\mathbf{e}_{ik} = \mathbf{0}), \quad \text{where}$$

$$\hat{Z}_j = \frac{\sum_{i=1}^{n}\sum_{k=1}^{n} Z_{ij} 1(\mathbf{e}_{ik} = \mathbf{0})}{\sum_{i=1}^{n}\sum_{k=1}^{n} 1(\mathbf{e}_{ik} = \mathbf{0})}. \tag{9}$$

The confluence covariance characterizes the covariance of flood index for all upstream link pairs.

A more targeted representation of the variability of flood index is through the confluence covariance for junctions of stream order $m$, which is given by

$$C_j(m) = \frac{\sum_{i=1}^{n}\sum_{k=1}^{n} (Z_{ij} - \hat{Z}_j)(Z_{kj} - \hat{Z}_j) 1(\mathbf{e}_{ik} = \mathbf{0}) 1(\omega_i = m) 1(\omega_k = m)}{\sum_{i=1}^{n}\sum_{k=1}^{n} 1(\mathbf{e}_{ik} = \mathbf{0}) 1(\omega_i = m) 1(\omega_k = m)}, \quad \text{where}$$

$$\hat{Z}_j = \frac{\sum_{i=1}^{n}\sum_{k=1}^{n} Z_{ij} 1(\mathbf{e}_{ik} = \mathbf{0}) 1(\omega_i = m) 1(\omega_k = m)}{\sum_{i=1}^{n}\sum_{k=1}^{n} 1(\mathbf{e}_{ik} = \mathbf{0}) 1(\omega_i = m) 1(\omega_k = m)}. \tag{10}$$

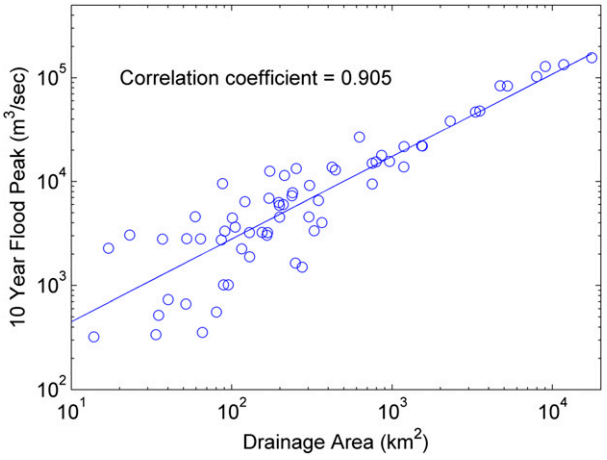


FIG. 2. Scaling properties of 10-yr flood peaks for 67 USGS gauging stations in Delaware River basin.

This quantity provides a scale-dependent representation of correlation of flood magnitudes.

The statistics introduced above provide useful tools for characterizing the aggregate distribution of flooding over a drainage network and representations of correlation structure of flood magnitudes over the network. Throughout the remainder of the paper, we will suppress dependence on storm $j$ whenever possible. Large samples of flood events can be used to characterize distributional properties of these quantities; in section 5 we point to methods of examining the climatology of tropical cyclone flooding.

## 3. Study area and flood summaries

### a. *Study area*

The Delaware River basin has a drainage area of 35 066 km$^2$ at Trenton, New Jersey, draining parts of Pennsylvania, New York, New Jersey, and Delaware to Delaware Bay. As shown in Fig. 1 (left), the upper basin is mountainous while the downstream portion of the watershed has lower relief. The basin is mostly forest covered, especially in mountainous areas, with modest urban development in low-elevation areas. There are four major tributaries of the Delaware River, the West Branch Delaware River, the East Branch Delaware River, the Lackawaxen River, and the Lehigh River.

Like most major rivers in the United States, the Delaware River is regulated by dams and reservoirs (Fig. 1, right). Reservoirs in the upper Delaware River basin are mainly operated for New York City water supply. Dams in the Lackawaxen and Lehigh River basins provide both flood control and water supply functions (Smith et al. 2010). Despite the extensive system of dams in the basin, the effects on flood hydrology are poorly understood (Williams and Wolman 1984; Batalla et al. 2004). Here we consider the effects of dams in the hydrologic model by treating them as low-pass filters. This is done by reducing channel velocity on links located with dams, that is, $v$ in Eq. (1), to 10% of its original value. This simple representation improves the overall performance of the model with minimal computational effort.

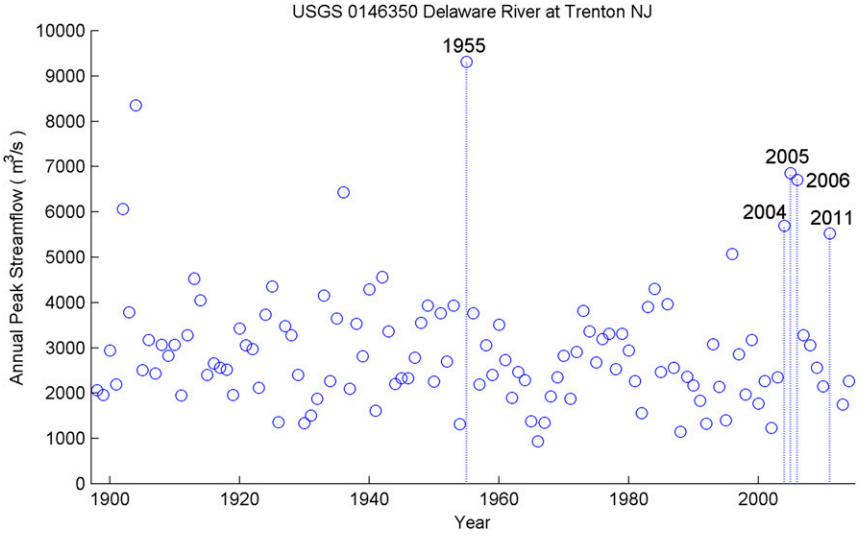


FIG. 3. Annual peak streamflow at Trenton.

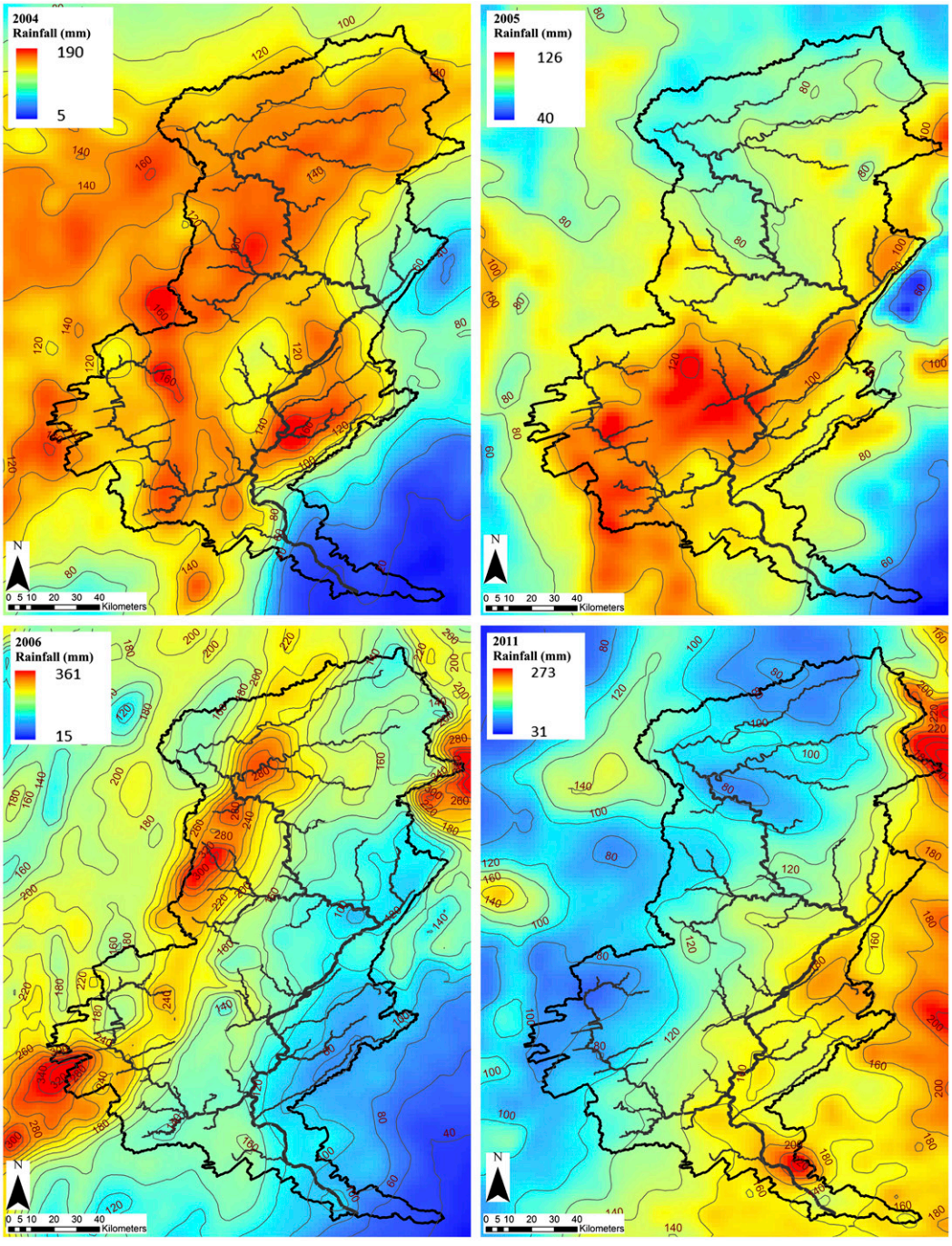


FIG. 4. Storm total rainfall accumulations with 20-mm interval contour for the (top left) 2004 storm (from 1000 UTC 17 Sep to 1000 UTC 19 Sep), (top right) 2005 storm (from 2300 UTC 31 Mar to 2300 UTC 2 Apr), (bottom left) 2006 storm (from 0900 UTC 25 Jun to 1900 UTC 28 Jun), and (bottom right) 2011 storm (from 0500 UTC 26 Aug to 0500 UTC 28 Aug).

The Delaware River basin is decomposed into 1891 links (Fig. 1, right) for hydrologic modeling. There are 67 USGS stream gauging stations in the study area, providing observations for hydrologic model validation and the computation of the $T$ (yr) flood. The 10-yr flood for the 67 observations exhibits a power-law relationship with the drainage area (with correlation of 0.905), as shown by the log–log plot in Fig. 2. With the estimated prefactor and exponent of the power-law relationship, we can compute the 10-yr flood magnitude for any drainage

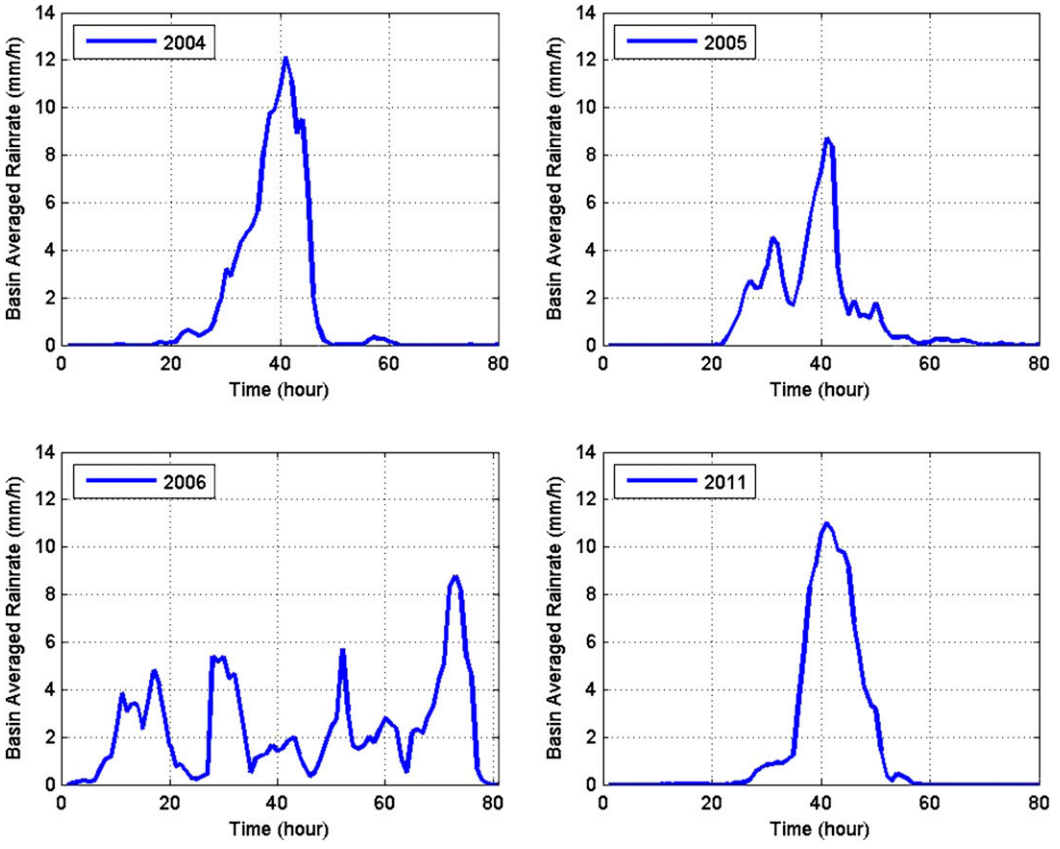


FIG. 5. Basin-averaged rainfall series for the (top left) 2004 storm (from 1000 UTC 17 Sep to 1000 UTC 19 Sep), (top right) 2005 storm (from 2300 UTC 31 Mar to 2300 UTC 2 Apr), (bottom left) 2006 storm (from 0900 UTC 25 Jun to 1900 UTC 28 Jun), and (bottom right) 2011 storm (from 0500 UTC 26 Aug to 0500 UTC 28 Aug).

area. Combining CUENCAS model simulations over a drainage network with computed values of 10-yr flood for any drainage area allows us to compute the flood index continuously over the network on an event basis.

### b. *Storms*

In this study, we examine four storm events that occurred 17–19 September 2004, 1–2 April 2005, 25–28 June 2006, and 26–28 August 2011, which resulted in the four largest flood peaks at the basin outlet (Trenton) since the flood in 1955 caused by Hurricanes Connie and Diane (Fig. 3).

Hurricane Ivan (2004) produced storm total rainfall accumulations ranging from 35 to 495 mm in the Delaware River basin as the storm center moved from west to east through the southern portion of the basin. The storm had weakened to a tropical depression before it affected the basin (from 1000 UTC 17 September to 1000 UTC 19 September) and completed extratropical transition by 1800 UTC 18 September (Stewart 2005). Hurricane Irene (2011) passed from south to north along the eastern margin of the basin and produced storm total rainfall accumulations ranging from 91 to 348 mm. The storm was a category 1 hurricane when it reached the Delaware River basin (from 0500 UTC 26 August to 0500 UTC 28 August) and decayed to a tropical storm after it passed the basin (0900 UTC 28 August; Avila and Cangialosi 2012). The storm began to undergo extratropical transition around 1200 UTC 27 August (Grumm 2011). Extratropical transition of Ivan and Irene, as with many tropical cyclone flood events in the northeastern United States, played a central role in heavy rainfall and flooding in Delaware River basin (Smith et al. 2010; Liu and Smith 2016).

The April 2005 flood event was associated with an extratropical cyclone. From 1200 UTC 2 April to 0600 UTC 3 April, the storm moved from northern Virginia to the northwestern corner of the Delaware River basin, with minimum sea level pressure decreasing from 995.5 to 981 hPa. Heavy rainfall was associated with a rapidly deepening cyclone, frontogenesis, and strong flow of moist air at 850 hPa (Smith et al. 2010).

The June 2006 flood was caused by heavy rainfall from warm season convective systems. The synoptic setting was characterized by a stationary midtropospheric trough over

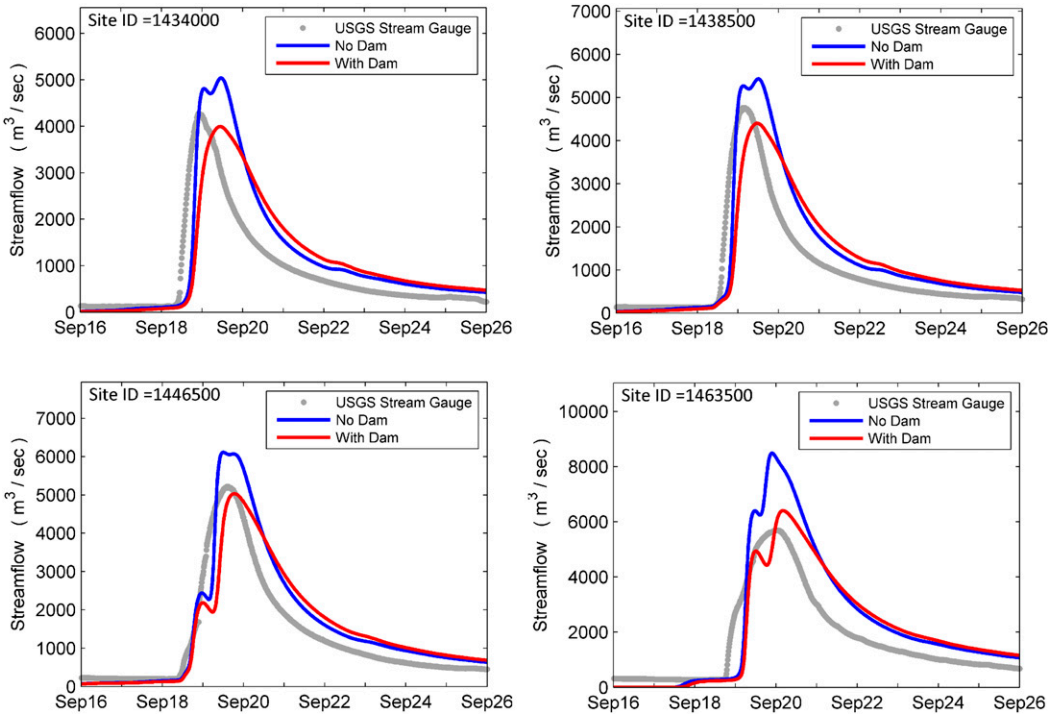


FIG. 6. Observed and simulated hydrographs at four sites on Delaware main stem for the 2004 event (location of four sites is shown in Fig. 1).

the Ohio Valley. The storm environment was characterized by a deep layer of humidity and large values of precipitable water. There was strong moisture transport in the lower atmosphere and heavy rainfall along the western margin of the Appalachians (Smith et al. 2010).

### c. *Rainfall distribution*

The southwest–northeast axis of the Appalachians shapes the rainfall distribution for all four storms (Fig. 4). For the 2004, 2005, and 2006 events, rainfall maxima were distributed along or to the west of the axis, while for the 2011 storm, extreme rainfall was located to the east of the axis. Although it is difficult to separate the contribution of orographic precipitation from other rainfall mechanisms, these patterns demonstrate the influence of complex terrain in modifying precipitation from the principal weather systems that produce major flooding in the basin. Other notable examples of weather systems that produce extreme rainfall along the eastern margin of the Appalachians include Hurricane Camille (1969) and Tropical Storm Allison (2001) (Javier et al. 2010). The connection between extreme rainfall and orographic precipitation mechanisms has been summarized in Smith (2006).

The spatial distribution of rainfall is strongly dependent on storm tracks (Smith 2006). The 2004 storm (Hurricane Ivan), for example, moved from west to east along the southern margin of the basin, producing strong upslope flow along the western slopes of the Appalachians. The 2011 storm (Hurricane Irene), however, moved from south to north along the eastern margin of the basin, producing strong upslope flow along the eastern margin of the Appalachians, resulting in heavy precipitation on the east side [see Lin et al. (1999) for similar features in Taiwan].

Time series of basin-averaged rain rate illustrate the intensity and duration of the four storms (Fig. 5). The 2004 and 2011 storms, both tropical cyclones, have rainfall concentrated in a 20-h window, with the peak basin-averaged rain rate of approximately 11–12 mm $h^{-1}$. The 2005 storm, an extratropical cyclone, had a longer duration (approximately 30 h), with a lower peak rain rate of approximately 9 mm $h^{-1}$. Rainfall from the 2006 warm season convective systems extended over 3 days, while the highest basin-averaged rain rate is similar to that of the 2005 storm. We will explore the linkage between flood distribution and the intensity and duration of the storms.

## 4. Flood index modeling results

The hydrologic model simulations are compared with discharge observations (typically at 15-min time resolution) from 67 USGS stream gauging stations across the basin.

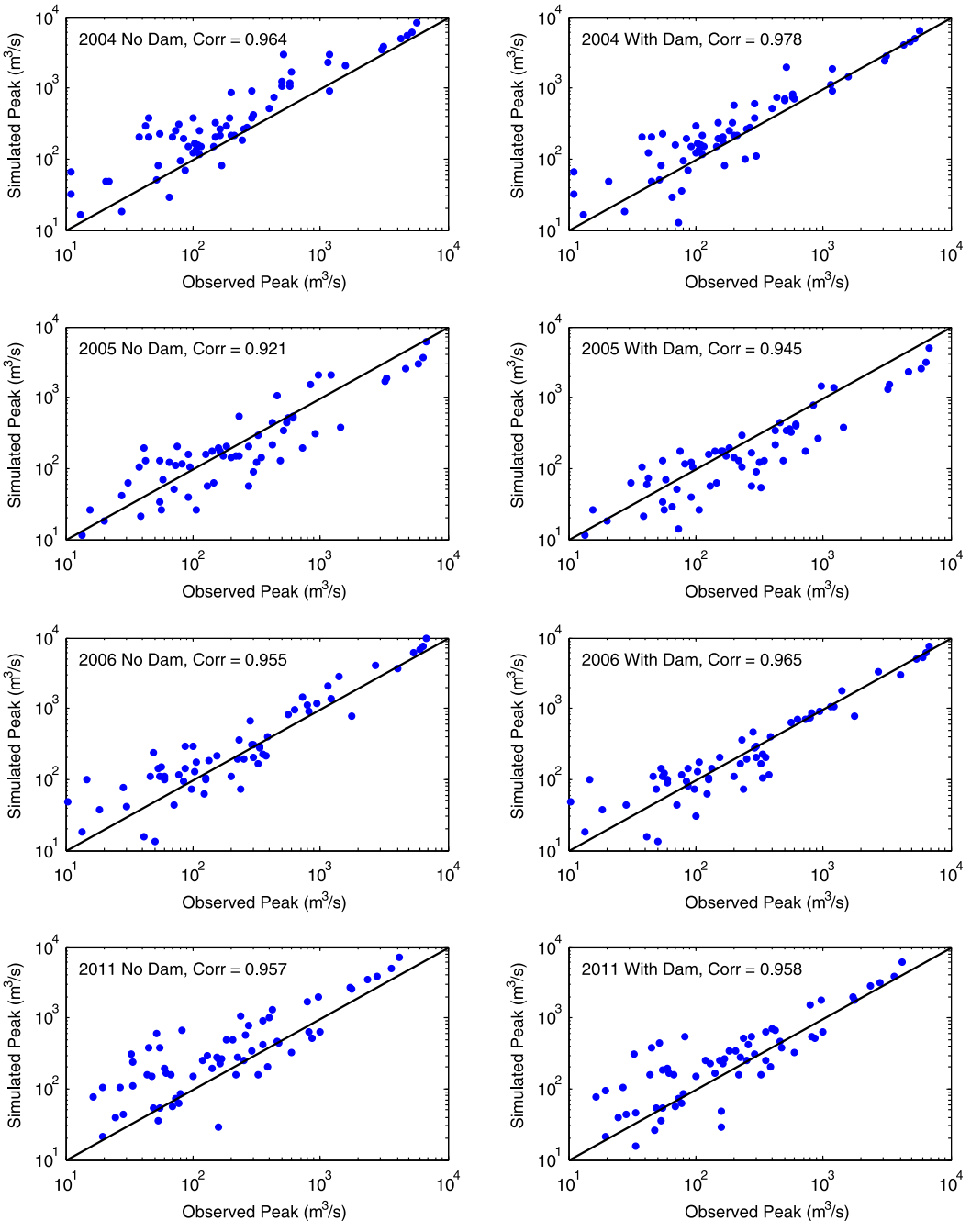


FIG. 7. Scatterplot of simulated and observed peaks at 67 USGS stream gauging stations for the (from top to bottom) 2004, 2005, 2006, and 2011 flood events.

Simulated hydrographs for the four storms generally compare well with observed hydrographs in terms of timing and peak magnitudes (see Fig. 6 for examples). The correlation coefficient between simulated and observed peaks is greater than 0.92 for all four storms (Fig. 7). Representation of dams, as described in the previous section, improves the performance of the model, increasing the correlation coefficient above 0.94 for all events. Sources of uncertainty in the model intercomparisons include errors in radar rainfall estimates, antecedent soil moisture, hydrologic model parameterization, and errors in discharge measurements (Javier et al. 2010; Villarini and Krajewski 2010; Mandapaka and Germann 2013; Domeneghetti et al. 2012; Le Coz 2012). As described in previous studies

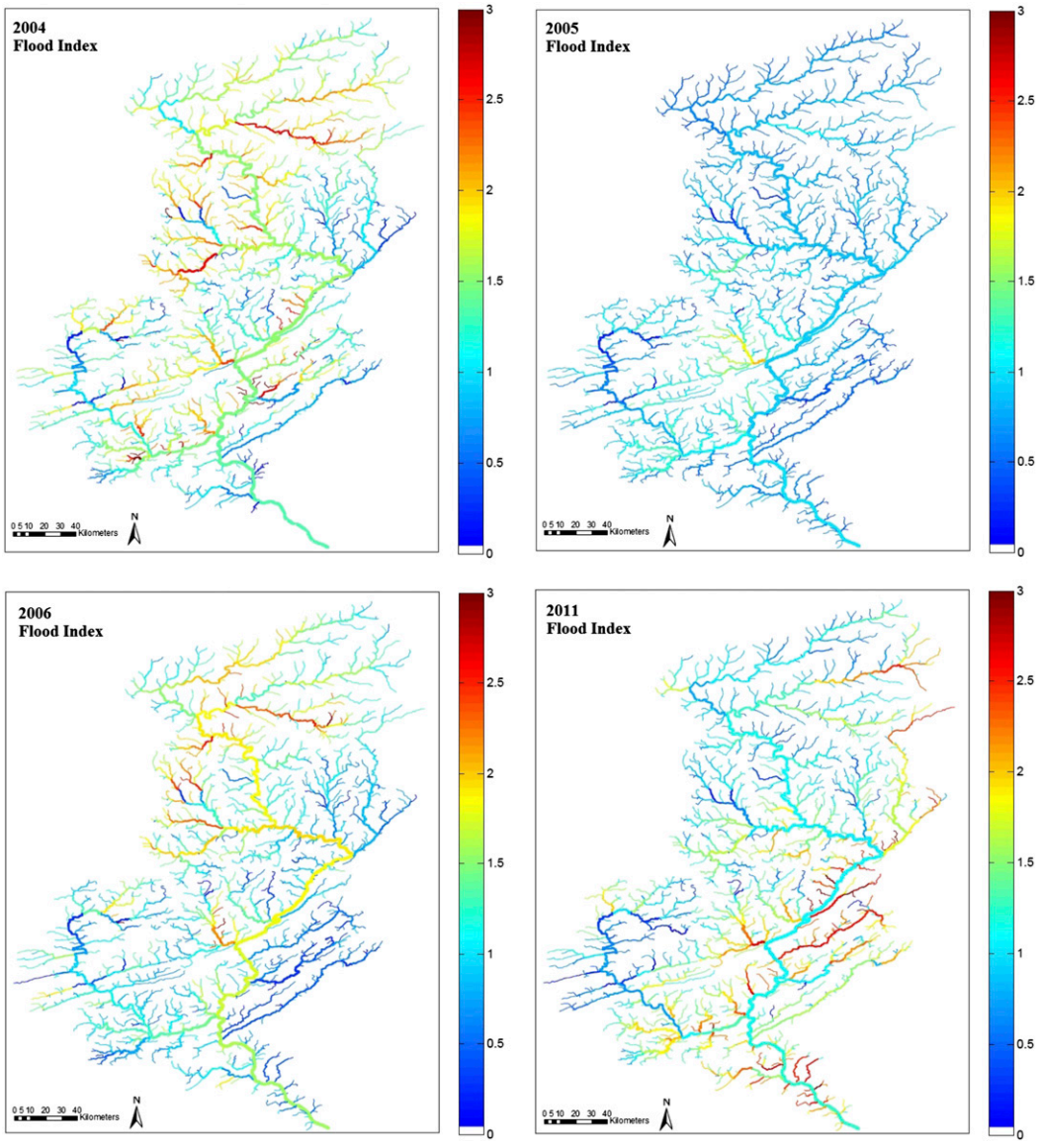


FIG. 8. Map of flood index for the (top left) 2004, (top right) 2005, (bottom left) 2006, and (bottom right) 2011 flood events.

(Ogden et al. 2000; Westrick and Mass 2001; Vieux and Bedient 2004; Smith et al. 2007), errors in the temporal and spatial distribution of rainfall are the leading determinants in hydrologic simulation uncertainties. Therefore, the most important improvement for hydrologic simulations is to have the best possible rainfall fields in time and space across different scales, as we will address in future work.

Despite having similar peak discharge values at the basin outlet at Trenton (Fig. 3), the distributions of flood magnitudes for the four flood events, as represented by the flood index in Fig. 8, vary markedly over the Delaware River basin. The 2005 event produced the largest flood peak at Trenton, 6853 $m^3 s^{-1}$, but had the most uniform distribution of flood index over the drainage basin. The 2004 and 2011 events produced smaller flood peaks at Trenton, 5522 and 5692 $m^3 s^{-1}$, respectively, but had flood index values that were more than twice as large as the peak flood index values for the 2005 event.

Figure 9 shows the box plots characterizing the central tendency (median), spread, and extremes of flood index values for the four storms. These results point to the relatively compact distribution of flood index values for the April 2005 storm and the relatively large number of outlier values for the September 2004 storm. Despite large variations in the mean flood index (Table 1), the

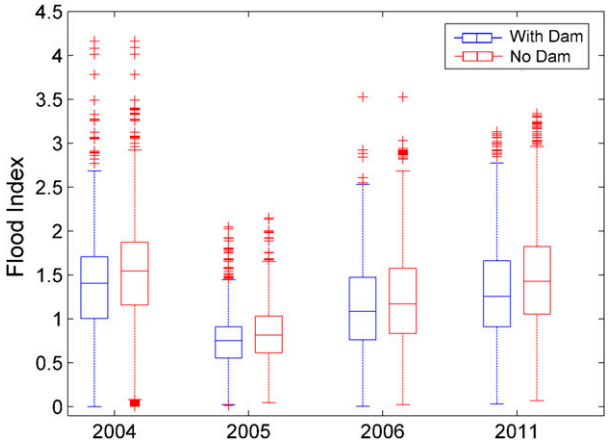


FIG. 9. Box plot of flood index for the four events.

coefficient of variation (standard deviation divided by the mean, Table 2) of flood index is relatively stable across storms, taking values of 0.45, 0.38, 0.47, and 0.45 for the 2004, 2005, 2006, and 2011 simulations with dams and values of 0.40, 0.36, 0.46, and 0.40 for the simulations without dams.

Regulation effects on annual flood peaks have been studied in various watersheds (Asquith 2001; Peters and Prowse 2001). Here we highlight in Fig. 9 the regulation effects on spatial distribution of event flood peaks over the Delaware River basin. For each of the storms, dams systematically reduce median values as well as the 0.25 and 0.75 quantiles of the flood index. Overall, there is only a modest change in the interquartile range, representing the spread of flood index values, but there is a pronounced decrease in extreme values of flood index for the 2011 flood, reflecting the occurrence of the most extreme rainfall in the Upper Delaware River basin, which includes watersheds controlled by water supply dams for New York City.

The contrasting distribution of flood index values over the Delaware River drainage network is clearly linked to the contrasting properties of the rainfall distribution of the four storms (Fig. 4). Large values of flood index are associated with areas of anomalously high storm accumulations, especially on small streams. For the 2004, 2006, and 2011 cases, we see high flood index values lying along a northeast–southwest axis; the location of the axis varies by storm, with high values for the 2004 and 2006 events concentrated in the western portion of the watershed and for the 2011 event in the eastern portion of the watershed. The spatial distribution of storm total accumulation, however, does not provide a comprehensive picture of flood magnitudes over the basin. For the 2004 event, rainfall accumulations exceeding 140 mm produced flood index values above 2 (similar to 2011 event), while similar storm total accumulations are associated with flood index values close to 1 for the 2006 storm. Rainfall–flood peak correlation will be discussed in more detail later in this section.

The fractional area function $I_j(z)$ of flood index values provides an effective tool for contrasting flood magnitudes over the Delaware River drainage network for the four flood events (Fig. 10). Despite having the largest peak at the outlet, the 2005 storm has lower flood magnitudes than the other three events over much of the drainage network. For the 2004, 2005, 2006, and 2011 events (simulated with dams), 70%, 16%, 52%, and 66% of the total channel length in the basin have flood index values greater than 1 (i.e., greater than the 10-yr flood).

The upper tail of flood index values exhibits sharp contrasts between the four events (Fig. 10, bottom). In particular, the 2005 event stands out for the relatively low values of flood index in the upper tail: 10% of the network has flood index values greater than a value slightly larger than 1. For the 2004, 2006, and 2011 events, the 10% exceedance values cluster around 2, that is, approximately 10% of the drainage network experienced flood peaks that were more than twice the 10-yr flood. For the 1% exceedance value, the 2006 flood is somewhat smaller than the two tropical cyclone floods in 2004 and 2011. Thus, the largest flood index values are associated with the two tropical cyclone floods.

The distribution of flood peaks over the drainage network varies systematically with Horton stream order (see Mantilla et al. 2006; Mandapaka et al. 2009; Menabde

TABLE 1. Mean of flood index for simulations with dam (WD) and no dam (ND).

| Mean | Total | Horton 1 | Horton 2 | Horton 3 | Horton 4 | Horton 5 | Horton 6 |
|---|---|---|---|---|---|---|---|
| 2004 WD | 1.28 | 1.42 | 1.04 | 1.40 | 1.05 | 1.37 | 0.97 |
| 2005 WD | 0.72 | 0.84 | 0.70 | 0.52 | 0.50 | 0.62 | 0.41 |
| 2006 WD | 1.07 | 1.23 | 0.86 | 1.24 | 0.89 | 0.58 | 0.46 |
| 2011 WD | 1.24 | 1.39 | 1.16 | 0.86 | 0.89 | 1.79 | 1.23 |
| 2004 ND | 1.44 | 1.71 | 1.07 | 1.42 | 1.06 | 1.41 | 1.02 |
| 2005 ND | 0.80 | 0.99 | 0.72 | 0.53 | 0.51 | 0.64 | 0.43 |
| 2006 ND | 1.19 | 1.45 | 0.88 | 1.26 | 0.90 | 0.60 | 0.48 |
| 2011 ND | 1.37 | 1.62 | 1.19 | 0.88 | 0.90 | 1.86 | 1.29 |

TABLE 2. Coefficient of variation for simulations with dam (WD) and no dam (ND).

| Coefficient of variation | Total | Horton 1 | Horton 2 | Horton 3 | Horton 4 | Horton 5 | Horton 6 |
|---|---|---|---|---|---|---|---|
| 2004 WD | 0.49 | 0.40 | 0.57 | 0.38 | 0.48 | 0.55 | 1.01 |
| 2005 WD | 0.43 | 0.35 | 0.42 | 0.38 | 0.32 | 0.46 | 0.60 |
| 2006 WD | 0.51 | 0.44 | 0.53 | 0.39 | 0.52 | 0.52 | 0.70 |
| 2011 WD | 0.48 | 0.41 | 0.50 | 0.45 | 0.50 | 0.39 | 0.50 |
| 2004 ND | 0.46 | 0.34 | 0.54 | 0.36 | 0.46 | 0.49 | 0.94 |
| 2005 ND | 0.43 | 0.31 | 0.39 | 0.36 | 0.31 | 0.40 | 0.53 |
| 2006 ND | 0.52 | 0.43 | 0.50 | 0.37 | 0.50 | 0.48 | 0.63 |
| 2011 ND | 0.44 | 0.34 | 0.47 | 0.43 | 0.48 | 0.33 | 0.43 |

et al. 2001; Gupta and Mesa 2014; Gupta et al. 2015). The distribution of flood index values shows a systematic increase in central tendency for Horton stream orders increasing from 1 to 3 (Fig. 11). This feature is characteristic of each storm and for both simulations with and without dams. Results for dam and no-dam simulations diverge significantly with the transition from stream order 3 to 4. For the no-dam simulations, the quantiles of flood index values generally increase for three of the four events; there is a slight decrease in the median and upper quantiles for the 2011 flood. For the simulations with dams, there is a marked decrease in flood index, for all quantiles, as we move from order 3 to 4 channel segments. The difference at the particular stream order follows from the fact that most river segments with Horton stream order 4 are downstream of dams (see Fig. 1, right). These results point to a systematic dependence of flood magnitudes on stream order and a systematic scale-based dependence of flood magnitude on reservoir impacts.

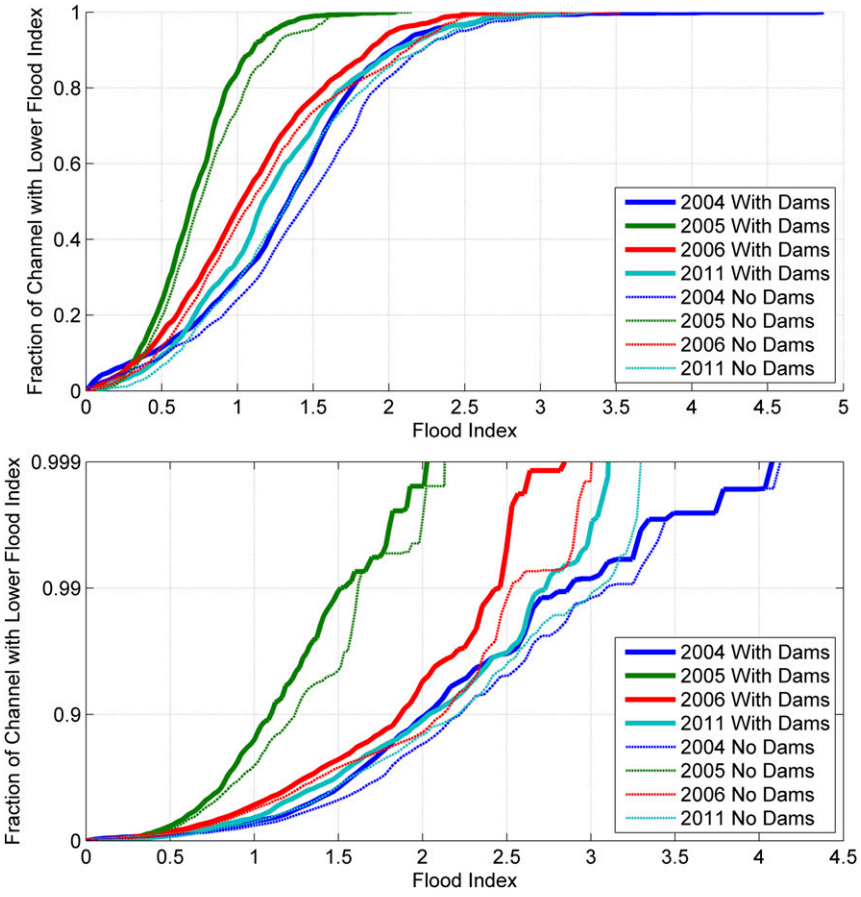


FIG. 10. Distribution of flood index over the entire river network in Delaware River basin where (bottom) gives a detailed look into tails in (top).

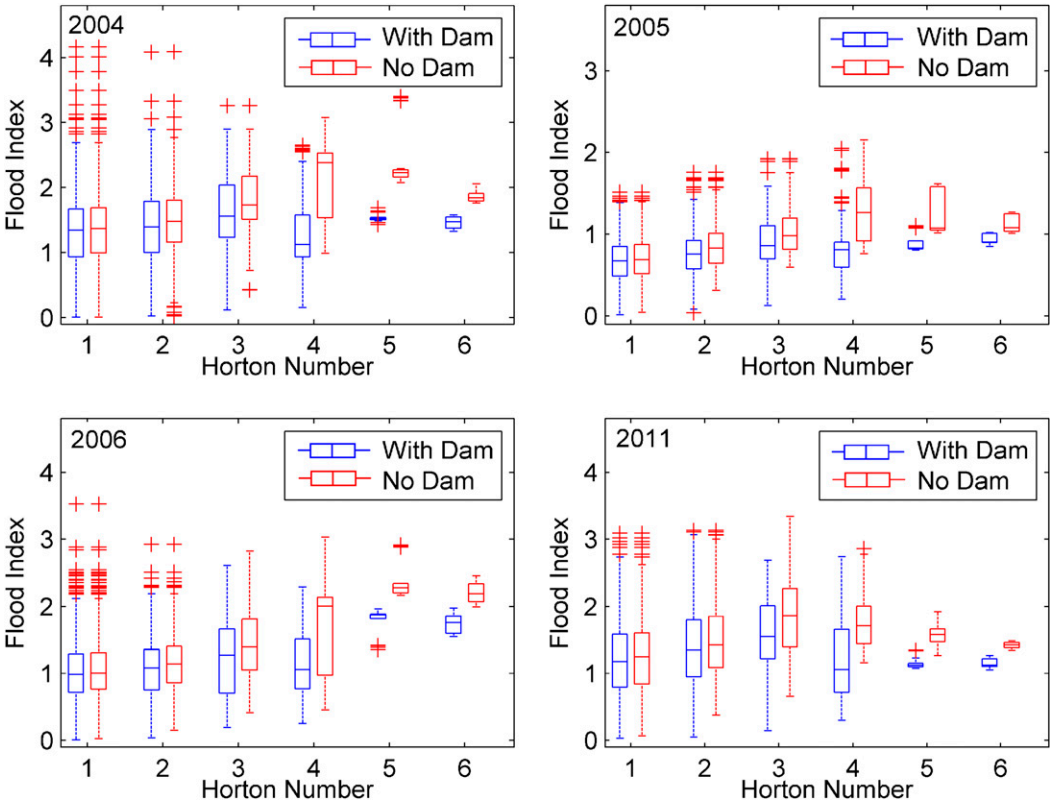


FIG. 11. Distribution of flood index by Horton stream order for the four events.

Flood magnitudes do not vary continuously over the drainage network; as we go from headwater to basin outlet, we see abrupt transitions of flood index with values gradually changing between the transitions. In Fig. 12, we show the downstream variation of flood magnitude along the main stem of the Delaware River, from its origin in the West Branch Delaware River to its outlet in Trenton, for the two tropical cyclone floods in September 2004 and September 2011. Anomalously large rainfall accumulations for both events were located in the headwaters of the Delaware River. For the 2011 event, a sharp spike in headwater flood index values is followed by a decay in flood index until an abrupt drop occurring at the West Branch Delaware River dam location (noted by ''Dam''). For the 2004 event, maximum flood index values are concentrated upstream of the West Branch Delaware River dam.

The largest increases in flood index for both events occur at the confluence of the West Branch and East Branch Delaware River (noted by ''A''). Abrupt transitions occur at major tributary junctions, notably the junction of the Lackawaxen River (in the middle basin, Lackawaxen) and Lehigh River (in the lower basin, ''B''). For the 2004 flood, there is an abrupt increase in flood index at the confluence of the Lackawaxen, reflecting the anomalously large rainfall in the subbasin (see Fig. 4) and an abrupt, but smaller, decrease in flood index occurs at the confluence of the Lehigh River (reflecting the relatively small rainfall accumulations in the subbasin). For the 2011 event, the change in flood index values at the Lackawaxen and Lehigh confluences are smaller.

As suggested by the preceding analyses, flood index values are correlated along the river network. Flood index values for the four storms remain stable on the Delaware River main stem (from Lackawaxen to Trenton; see Figs. 8 and 12a), where we use Pearson correlation to examine downstream influence, with Lackawaxen as the starting point (Fig. 13). As expected, the correlation decreases with separation distance for all four storms. For the 2006 and 2004 floods (with flood index on main stream varying from 2 to 1.3), the correlation over a distance of 50 km downstream is as high as 0.94. For the 2011 and 2005 events (with flood index varying from 1.3 to 0.8), the correlation over a distance of 50 km drops to 0.65. For these events, larger flood index values are associated with stronger downstream correlation. The change of flood peak along the stream is a combined effect of attenuation and aggregation of flows. While the flood peak attenuation is complicated,

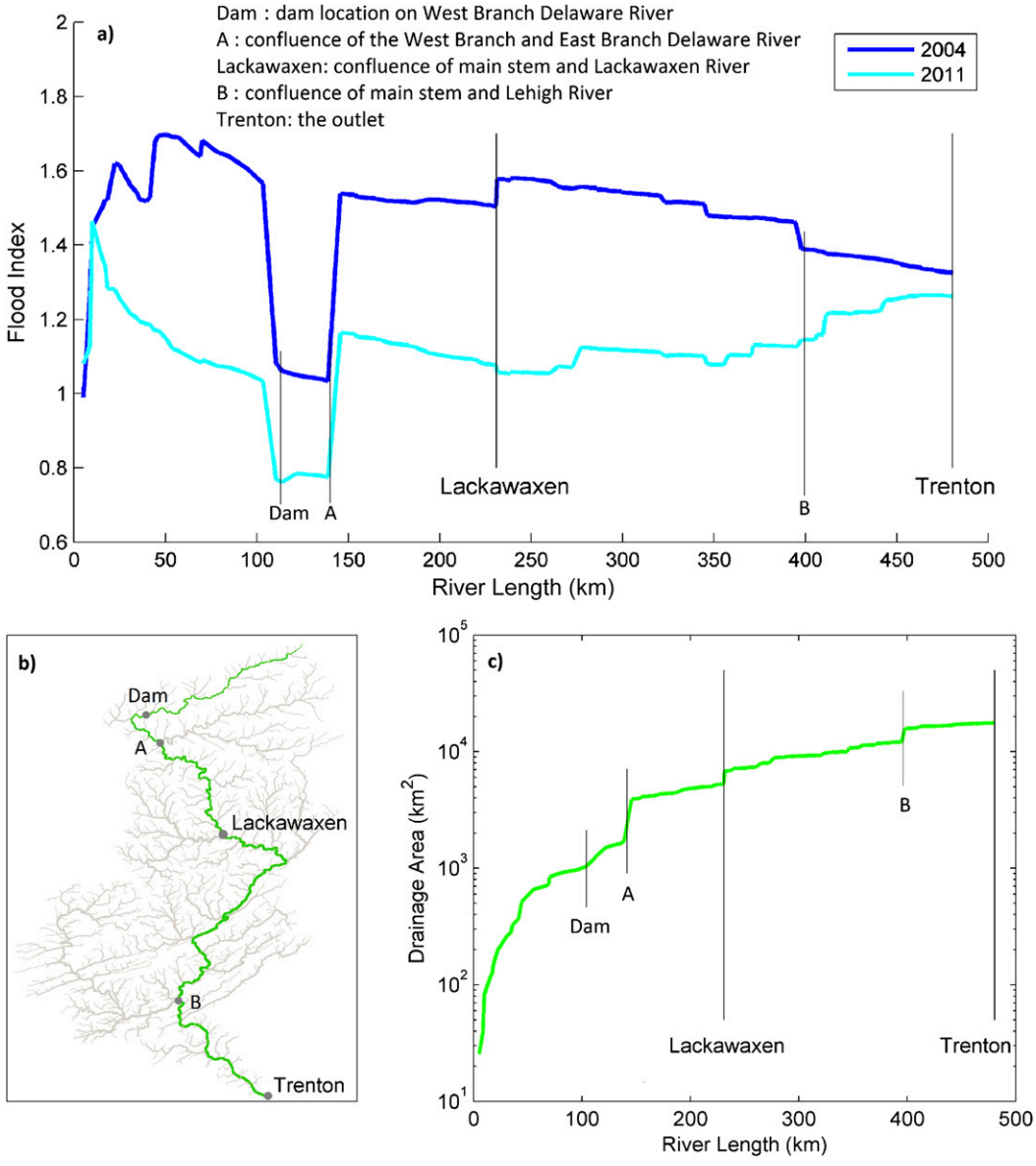


FIG. 12. (a) Downstream variation of flood index along the main stem of Delaware River, from its origin in the West Branch Delaware River to its outlet in Trenton. (b) The main stem of Delaware River. (c) Change of drainage area along the main stem of Delaware River.

the change caused by confluence of streams is smaller with larger floods (higher flood index). This feature is linked to the higher downstream correlation with larger values of flood index. This spatial correlation of the flood index, however, is also highly influenced by the spatial correlation of the rainfall fields.

The confluence covariance statistics also provide information about the storm-to-storm variation of flood peak distributions. In Table 3, we present the confluence correlation statistics (covariance divided by variance) for streams of order 1, 2, and 3 (sample size is too small to develop useful statistics for higher stream orders). The smallest correlation, 0.23, is for third-order streams with Hurricane Irene (2011) for simulations with dams. The correlation increases to 0.60 for third-order streams in Irene simulations without dams. The highest correlations for third-order streams are for the April 2005 extratropical flood event, 0.79 with dams and 0.82 with no dams. For the June 2006 convective event, correlation increases for third-order streams from 0.54 without dams to 0.62 with dams. The June 2006 event has the largest correlations for first-order streams, 0.71 for

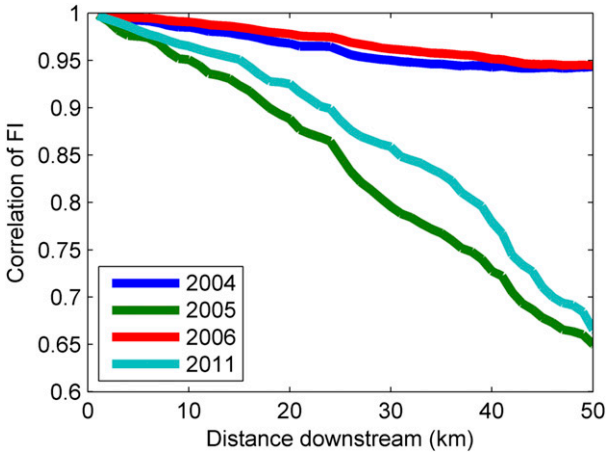


FIG. 13. Spatial correlations of flood index (FI) downstream along Delaware main stem between Lackawaxen and Trenton.

simulations with and without dams. The smallest correlations for first-order streams are for the 2011 flood, with values of 0.49 without dams and 0.56 with dams. There is not a systematic dependence of confluence correlation on stream order. Confluence correlation statistics provide a useful tool for assessing the effects of rainfall variability in time and space for a particular event (as discussed below) on the spatial structure of flood magnitudes. They also provide insight to the role of dams on the stream order dependence of flood magnitudes.

As noted above, the distribution of flood index is significantly linked to the distribution of rainfall. In Figs. 14 and 15, we summarize the distribution of rainfall over the Delaware River basin based on storm total rainfall, maximum hourly rain rate, and maximum 24-h rainfall rate (i.e., hourly rain rate for each grid in a 24-h period centered at the time of the maxima of basin-averaged rainfall rate). These rainfall distributions are compared to the distribution of flood index (Figs. 9, 10) to explore the role of rainfall properties in determining flood magnitudes. Although maps of storm total accumulations (Fig. 4) provide useful insights to the spatial distribution of flood index (Fig. 8), the distribution of storm total accumulations does not provide a comprehensive characterization of flood potential over the drainage network. The 2005 storm has the most extreme storm total accumulations and the 2004 storm has the least extreme, which is opposite of the distribution of flood index. In Figs. 9 and 10, the 2005 flood stands out much weaker than the other three, and the 2004 flood is the most extreme among the four. The distributions of peak hourly and 24-h rainfall rates clearly distinguish the 2005 storm from the others as the least extreme and 2004 storm as the most extreme in terms of central tendency and extremes.

TABLE 3. Confluence correlation for simulations with dam (WD) and no dam (ND).

| Confluence correlation | Horton 1 | Horton 2 | Horton 3 |
|---|---|---|---|
| 2004 WD | 0.65 | 0.75 | 0.55 |
| 2005 WD | 0.66 | 0.67 | 0.79 |
| 2006 WD | 0.71 | 0.64 | 0.62 |
| 2011 WD | 0.56 | 0.55 | 0.23 |
| 2004 ND | 0.66 | 0.77 | 0.60 |
| 2005 ND | 0.64 | 0.64 | 0.82 |
| 2006 ND | 0.71 | 0.62 | 0.54 |
| 2011 ND | 0.49 | 0.52 | 0.60 |

The distribution of hourly rainfall rates, especially in their upper tail, highlight contrasts in the upper tail of flood index distributions, not just between the 2005 flood and the other three events, but also among the 2006, 2004, and 2011 events. The relative high frequency of extreme hourly rainfall rates for the 2004 storm drives the relatively high fraction of flood index values exceeding 3, which indicates that a key issue for assessing spatial structure of extreme flooding using radar rainfall fields and hydrologic models is determining the accuracy of rainfall estimates for the most extreme rainfall rates.

## 5. Summary and conclusions

In this study, we develop a framework to characterize the distribution of flood magnitudes over large river networks. Flood magnitudes are characterized by the flood index, which is defined as the ratio of the peak magnitude of a flood event to the historical 10-yr flood magnitude. Flood peaks are computed continuously over the drainage network using a distributed hydrologic model, CUENCAS, with high-resolution radar rainfall fields as the principal forcing. The magnitudes of 10-yr flood are computed as power-law functions of drainage area, with empirical coefficients of the power-law relationship developed from regional flood peak data. Summary statistics for characterizing probability distribution and spatial correlation of flood magnitudes over the drainage network for a flood event are developed based on the dimensionless flood index.

This framework is applied to four storm events in the Delaware River basin in the northeastern United States. The four storms, which occurred 17–19 September 2004, 1–2 April 2005, 25–28 June 2006, and 26–28 August 2011, resulted in the four largest flood peaks at the Delaware basin outlet since the flood of record in 1955 caused by Hurricanes Connie and Diane. The four floods reflect the principal flood-generating mechanisms in the eastern United States: landfalling tropical cyclones (September 2004 caused by Hurricane Ivan and

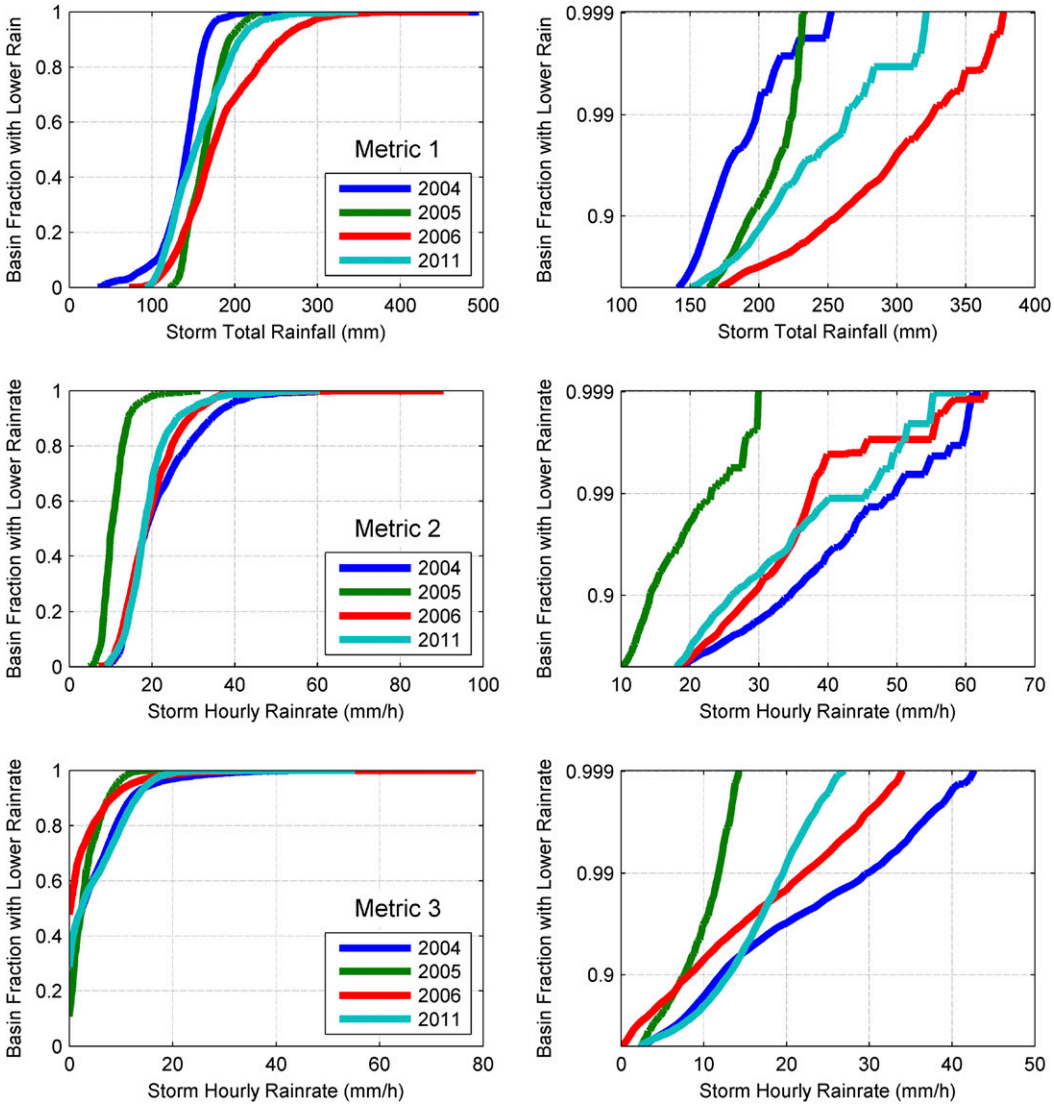


FIG. 14. Distribution of storm total rainfall accumulations for each grid (metric 1; same values as shown in Figs. 4–7), max hourly rain rate for each grid during the entire storm (metric 2), and hourly rain rate for each grid in a 24-h period centered at the time of the maxima of basin-averaged rainfall rate (metric 3). Closer looks into tails are shown in panels on the right.

August 2011 caused by Hurricane Irene), late winter/early spring extratropical systems (April 2005), and warm season convective systems (June 2006).

Despite having similar peak discharge values at the basin outlet, the distributions of flood magnitudes over the drainage network vary markedly for the September 2004, April 2005, June 2006, and September 2011 flood events. The distributions of flood magnitudes also vary markedly in the upper tail, with the April 2005 event having the most tightly concentrated distribution of flood magnitudes and ''lightest'' upper tail.

The distribution of flood index values shows a systematic increase in central tendency for Horton stream orders increasing from 1 to 3. This feature is characteristic of each storm and for simulations with and without dams. Results for dam and no-dam simulations diverge significantly with the transition from stream order 3 to 4. These results point to a systematic dependence of flood magnitudes on stream order and a systematic scale-based dependence of flood magnitude on reservoir impacts. Dams systematically reduce flood magnitudes over the drainage network. Representation of dams provides the capability of capturing the local impact of dams for storm events, such as the September 2011 tropical cyclone event, which concentrate extreme rainfall in portions of the watershed controlled by dams.

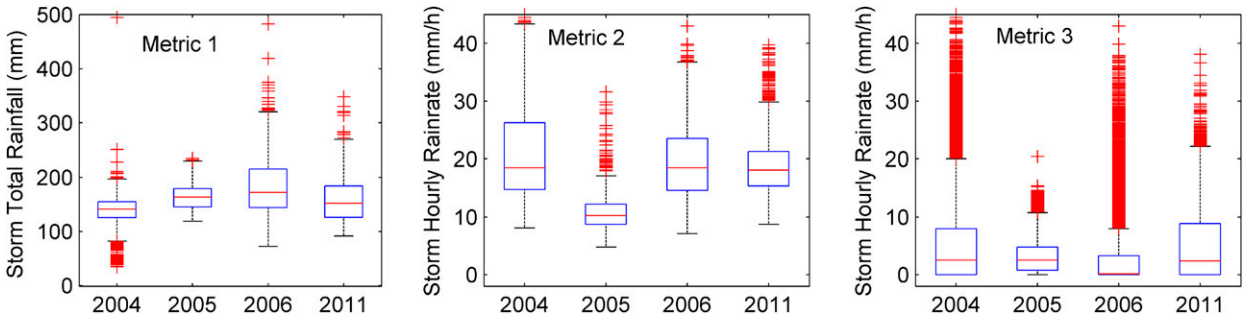


FIG. 15. Box plot of storm total rainfall accumulations for each grid (metric 1; same values as shown in Fig. 4), max hourly rain rate for each grid during the entire storm (metric 2), and hourly rain rate for each grid in a 24-h period centered at the time of the maxima of basin-averaged rainfall rate (metric 3).

The spatial correlation of flood index along the main stem reaches 0.94 for a downstream distance of 50 km for the 2004 and 2006 floods (flood index varying from 1.3 to 2 on the main stem) and is only 0.65 for the 2005 and 2011 floods (flood index varying from 0.8 to 1.3 on the main stem). For the sample of flood events, higher values of flood index are linked to stronger downstream correlation.

Confluence covariance statistics provide useful information about the storm-to-storm variation of flood peak distributions over the drainage network. Results for the sample of four storms show sharp contrasts in confluence correlation from storm to storm and with stream order. These statistics provide important tools for assessing the role of rainfall variability on flood response and in assessing the dependence of dams on stream order.

In terms of storm total rainfall accumulations as well as the flood peak at the basin outlet, the 2005 extratropical event is the most extreme, while the 2004 and 2011 tropical cyclone events are the least extreme. The 2005 storm, however, produces lower flood magnitudes than the other three over much of the drainage network, while the 2004 and 2011 events produce the most extreme values of flood index. This difference is associated with contrasting spatial structure of rainfall and contrasting rainfall-rate distributions within the storms. Maximum hourly rain-rate distributions over the watershed distinguish the 2005 from the 2004 and 2011 events.

The flood index framework introduced in this study can be utilized to characterize the spatial distribution of floods, especially those caused by landfalling tropical cyclones. Future work will apply this framework to large numbers of tropical cyclone rainfall events to assess and characterize the associated long-term flood hazards. For both historic analyses and future projections, the most important improvement for hydrologic simulations is to have the best possible rainfall fields in time and space across different scales. This goes along with our current research on a simple, physics-based rainfall model that can be coupled with a large number of synthetic tropical cyclones (Emanuel et al. 2006, 2008; Zhu et al. 2013). This study fits into our long-term goal of developing a methodology to quantify the risk of inland flooding associated with landfalling tropical cyclones.

*Acknowledgments.* This material is based upon work supported by the National Science Foundation under Grant EAR-1520683. We would also like to thank Luciana K. Cunha and Mary Lynn Baeck for their generous help with the hydrological modeling.

## REFERENCES

Asquith, W. H., 2001: Effects of regulation on L-moments of annual peak streamflow in Texas. USGS Water-Resources Investigations Rep. 01-4243, 66 pp. [Available online at https://pubs.usgs.gov/wri/wri014243/pdf/wri01-4243-new.pdf.]

Avila, L. A., and J. Cangialosi, 2012: Tropical cyclone report: Hurricane Irene (AL092011), 21–28 August 2011. NHC Tech. Rep., 45 pp. [Available online at http://www.nhc.noaa.gov/data/tcr/AL092011_Irene.pdf.]

Ayalew, T. B., 2015: Physical basis of the power-law spatial scaling structure of peak discharges. Ph.D. thesis, The University of Iowa, 286 pp. [Available online at http://ir.uiowa.edu/etd/1537/.]

——, W. F. Krajewski, and R. Mantilla, 2014a: Connecting the power-law scaling structure of peak-discharges to spatially variable rainfall and catchment physical properties. *Adv. Water Resour.*, **71**, 32–43, doi:10.1016/j.advwatres.2014.05.009.

——, ——, ——, and S. J. Small, 2014b: Exploring the effects of hillslope–channel link dynamics and excess rainfall properties on the scaling structure of peak-discharge. *Adv. Water Resour.*, **64**, 9–20, doi:10.1016/j.advwatres.2013.11.010.

Batalla, R. J., C. M. Gomez, and G. M. Kondolf, 2004: Reservoir-induced changes in the Ebro River basin (NE Spain). *J. Hydrol.*, **290**, 117–136, doi:10.1016/j.jhydrol.2003.12.002.

Blöschl, G., and Coauthors, 2007: At what scale do climate variability and land cover change impact on flooding and low

flows? *Hydrol. Processes*, **21**, 1241–1247, doi:10.1002/hyp.6669.

——, T. Nester, J. Komma, J. Parajka, and R. A. Perdigao, 2013: The June 2013 flood in the Upper Danube basin, and comparisons with the 2002, 1954 and 1899 floods. *Hydrol. Earth Syst. Sci.*, **17**, 5197–5212, doi:10.5194/hess-17-5197-2013.

Cunha, L. K., 2012: Exploring the benefits of satellite remote sensing for flood prediction across scales. Ph.D. thesis, The University of Iowa, 245 pp. [Available online at http://ir.uiowa.edu/etd/2848/.]

——, P. V. Mandapaka, W. F. Krajewski, R. Mantilla, and A. A. Bradley, 2012: Impact of radar-rainfall error structure on estimated flood magnitude across scales: An investigation based on a parsimonious distributed hydrological model. *Water Resour. Res.*, **48**, W10515, doi:10.1029/2012WR012138.

Czajkowski, J., G. Villarini, E. Michel-Kerjan, and J. A. Smith, 2013: Determining tropical cyclone inland flooding loss on a large scale through a new flood peak ratio-based methodology. *Environ. Res. Lett.*, **8**, 044056, doi:10.1088/1748-9326/8/4/044056.

——, ——, M. Montgomery, E. Michel-Kerjan, and R. Goska, 2017: Assessing current and future freshwater flood risk from North Atlantic tropical cyclones via insurance claims. *Sci. Rep.*, **7**, 41609, doi:10.1038/srep41609.

Domeneghetti, A., A. Castellarin, and A. Brath, 2012: Assessing rating-curve uncertainty and its effects on hydraulic model calibration. *Hydrol. Earth Syst. Sci.*, **16**, 1191–1202, doi:10.5194/hess-16-1191-2012.

Durbude, D. G., M. K. Jain, and S. K. Mishra, 2011: Long-term hydrologic simulation using SCS-CN-based improved soil moisture accounting procedure. *Hydrol. Processes*, **25**, 561–579, doi:10.1002/hyp.7789.

Emanuel, K., S. Ravela, E. Vivant, and C. Risi, 2006: A statistical deterministic approach to hurricane risk assessment. *Bull. Amer. Meteor. Soc.*, **87**, 299–314, doi:10.1175/BAMS-87-3-299.

——, R. Sundararajan, and J. Williams, 2008: Hurricanes and global warming: Results from downscaling IPCC AR4 simulations. *Bull. Amer. Meteor. Soc.*, **89**, 347–367, doi:10.1175/BAMS-89-3-347.

Falcone, J., 2011: GAGES-II: Geospatial attributes of gages for evaluating streamflow geospatial data presentation form: Vector digital data. USGS, accessed 17 March 2016. [Available online at http://water.usgs.gov/GIS/metadata/usgswrd/XML/gagesII_Sept2011.xml.]

Goel, N. K., S. M. Seth, and S. Chandra, 1998: Multivariate modeling of flood flows. *J. Hydraul. Eng.*, **124**, 146–155, doi:10.1061/(ASCE)0733-9429(1998)124:2(146).

Grumm, R. H., 2011: Irene rains over the East Coast. Tech. Doc., 30 pp. [Available online at http://cms.met.psu.edu/sref/severe/2011/28Aug2011.pdf.]

Gupta, V. K., and O. J. Mesa, 2014: Horton laws for hydraulic–geometric variables and their scaling exponents in self-similar river networks. *Nonlinear Processes Geophys.*, **21**, 1007–1025, doi:10.5194/npg-21-1007-2014.

——, T. B. Ayalew, R. Mantilla, and W. F. Krajewski, 2015: Classical and generalized Horton laws for peak flows in rainfall–runoff events. *Chaos*, **25**, 075408, doi:10.1063/1.4922177.

Javier, J. R. N., J. A. Smith, M. L. Baeck, and G. Villarini, 2010: Flash flooding in the Philadelphia metropolitan region. *J. Hydrol. Eng.*, **15**, 29–38, doi:10.1061/(ASCE)HE.1943-5584.0000148.

Krstanovic, P. F., and V. P. Singh, 1987: A multivariate stochastic flood analysis using entropy. *Hydrologic Frequency Modeling*, V. P. Singh, Ed., D. Reidel, 515–539, doi:10.1007/978-94-009-3953-0_37.

Laaha, G., J. O. Skøien, and G. Blöschl, 2012: Comparing geostatistical models for river networks. *Geostatistics Oslo 2012*, P. Abrahamsen, R. Hauge, and O. Kolbjørnsen, Eds., Quantitative Geology and Geostatistics, Vol. 17, Springer, 543–553, doi:10.1007/978-94-007-4153-9_44.

Le Coz, J., 2012: A literature review of methods for estimating the uncertainty associated with stage–discharge relations. WMO Tech. Doc. PO6a, 21 pp. [Available online at http://www.wmo.int/pages/prog/hwrp/Flow/flow_tech/documents/WMO_PO6a_RC_uncertainty.pdf.]

Lin, Y.-L., J. Han, D. W. Hamilton, and C. Y. Huang, 1999: Orographic influence on a drifting cyclone. *J. Atmos. Sci.*, **56**, 534–562, doi:10.1175/1520-0469(1999)056<0534:OIOADC>2.0.CO;2.

Liu, M., and J. Smith, 2016: Extreme rainfall from landfalling tropical cyclones in the eastern United States: Hurricane Irene (2011). *J. Hydrometeor.*, **17**, 2883–2904, doi:10.1175/JHM-D-16-0072.1.

Mandapaka, P. V., and U. Germann, 2013: Radar-rainfall error models and ensemble generators. *Rainfall: State of the Science*, *Geophys. Monorgr.*, Vol. 191, Amer. Geophys. Union, 247–264.

——, W. F. Krajewski, G. J. Ciach, G. Villarini, and J. A. Smith, 2009: Estimation of radar-rainfall error spatial correlation. *Adv. Water Resour.*, **32**, 1020–1030, doi:10.1016/j.advwatres.2008.08.014.

Mantilla, R., 2007: Physical basis of statistical scaling in peak flows and stream flow hydrographs for topologic and spatially embedded random self-similar channel networks. Ph.D. thesis, University of Colorado, 144 pp. [Available online at http://www.iihr.uiowa.edu/rmantilla/files/2015/03/Thesis_Mantilla.pdf.]

——, and V. K. Gupta, 2005: A GIS numerical framework to study the process basis of scaling statistics in river networks. *IEEE Geosci. Remote Sens. Lett.*, **2**, 404–408, doi:10.1109/LGRS.2005.853571.

——, ——, and O. J. Mesa, 2006: Role of coupled flow dynamics and real network structures on Hortonian scaling of peak flows. *J. Hydrol.*, **322**, 155–167, doi:10.1016/j.jhydrol.2005.03.022.

Menabde, M., S. Veitzer, V. Gupta, and M. Sivapalan, 2001: Tests of peak flow scaling in simulated self-similar river networks. *Adv. Water Resour.*, **24**, 991–999, doi:10.1016/S0309-1708(01)00043-4.

Merz, R., G. Blöschl, and G. Humer, 2008: National flood discharge mapping in Austria. *Nat. Hazards*, **46**, 53–72, doi:10.1007/s11069-007-9181-7.

Michel, C., V. Andréassian, and C. Perrin, 2005: Soil Conservation Service Curve Number method: How to mend a wrong soil moisture accounting procedure? *Water Resour. Res.*, **41**, W02011, doi:10.1029/2004WR003191.

Mishra, S., and V. Singh, 1999: Another look at SCS-CN method. *J. Hydrol. Eng.*, **4**, 257–264, doi:10.1061/(ASCE)1084-0699(1999)4:3(257).

Moser, B. A., W. A. Gallus Jr., and R. Mantilla, 2015: An initial assessment of radar data assimilation on warm season rainfall forecasts for use in hydrologic models. *Wea. Forecasting*, **30**, 1491–1520, doi:10.1175/WAF-D-14-00125.1.

NRCS, 1986: Urban hydrology for small watersheds. USDA TR-55, 164 pp. [Available online at https://www.nrcs.usda.gov/Internet/FSE_DOCUMENTS/stelprdb1044171.pdf.]

Ogden, F., H. Sharif, S. Senarath, J. Smith, M. Baeck, and J. Richardson, 2000: Hydrologic analysis of the Fort Collins, Colorado, flash flood of 1997. *J. Hydrol.*, **228**, 82–100, doi:10.1016/S0022-1694(00)00146-3.

Paik, K., and P. Kumar, 2004: Hydraulic geometry and the nonlinearity of the network instantaneous response. *Water Resour. Res.*, **40**, W03602, doi:10.1029/2003WR002821.

Peters, D. L., and T. D. Prowse, 2001: Regulation effects on the lower Peace River, Canada. *Hydrol. Processes*, **15**, 3181–3194, doi:10.1002/hyp.321.

Ponce, V. M., and R. H. Hawkins, 1996: Runoff curve number: Has it reached maturity? *J. Hydrol. Eng.*, **1**, 11–19, doi:10.1061/(ASCE)1084-0699(1996)1:1(11).

Sackl, B., and H. Bergmann, 1987: A bivariate flood model and its application. *Hydrol. Freq. Model.*, **31**, 571–582, doi:10.1007/978-94-009-3953-0_40.

Sivapalan, M., 2003: Process complexity at hillslope scale, process simplicity at the watershed scale: Is there a connection? *Hydrol. Processes*, **17**, 1037–1041, doi:10.1002/hyp.5109.

——, K. Beven, and E. F. Wood, 1987: On hydrologic similarity: 2. A scaled model of storm runoff production. *Water Resour. Res.*, **23**, 2266–2278, doi:10.1029/WR023i012p02266.

Skøien, J. O., R. Merz, and G. Blöschl, 2005: Top-kriging—Geostatistics on stream networks. *Hydrol. Earth Syst. Sci.*, **2**, 277–287, doi:10.5194/hess-10-277-2006.

Smith, J. A., M. L. Baeck, K. L. Meierdiercks, A. J. Miller, and W. F. Krajewski, 2007: Radar rainfall estimation for flash flood forecasting in small urban watersheds. *Adv. Water Resour.*, **30**, 2087–2097, doi:10.1016/j.advwatres.2006.09.007.

——, ——, G. Villarini, and W. F. Krajewski, 2010: The hydrology and hydrometeorology of flooding in the Delaware River basin. *J. Hydrometeor.*, **11**, 841–859, doi:10.1175/2010JHM1236.1.

Smith, R. B., 2006: Progress on the theory of orographic precipitation. *Spec. Pap. Geol. Soc. Amer.*, **398**, 1–16, doi:10.1130/2006.2398(01).

Stedinger, J. R., 1983: Estimating a regional flood frequency distribution. *Water Resour. Res.*, **19**, 503–510, doi:10.1029/WR019i002p00503.

——, and G. D. Tasker, 1985: Regional hydrologic analysis: 1. Ordinary, weighted, and generalized least squares compared. *Water Resour. Res.*, **21**, 1421–1432, doi:10.1029/WR021i009p01421.

——, and ——, 1986: Regional hydrologic analysis: 2. Model-error estimators, estimation of sigma and log-Pearson type 3 distributions. *Water Resour. Res.*, **22**, 1487–1499, doi:10.1029/WR022i010p01487.

Stewart, S. R., 2005: Tropical cyclone report: Hurricane Ivan (AL092004). NHC Tech. Rep., 44 pp. [Available online at http://www.nhc.noaa.gov/data/tcr/AL092004_Ivan.pdf.]

Vieux, B. E., and P. B. Bedient, 2004: Assessing urban hydrologic prediction accuracy through event reconstruction. *J. Hydrol.*, **299**, 217–236, doi:10.1016/S0022-1694(04)00366-X.

Villarini, G., and W. F. Krajewski, 2010: Sensitivity studies of the models of radar-rainfall uncertainties. *J. Appl. Meteor. Climatol.*, **49**, 288–309, doi:10.1175/2009JAMC2188.1.

——, and J. A. Smith, 2010: Flood peak distributions for the eastern United States. *Water Resour. Res.*, **46**, W06504, doi:10.1029/2009WR008395.

Westrick, K. J., and C. F. Mass, 2001: An evaluation of a high-resolution hydrometeorological modeling system for prediction of a cool-season flood event in a coastal mountainous watershed. *J. Hydrometeor.*, **2**, 161–180, doi:10.1175/1525-7541(2001)002<0161:AEOAHR>2.0.CO;2.

Williams, G. P., and M. G. Wolman, 1984: Downstream effects of dams on alluvial rivers. Geological Survey Prof. Paper 1286, 83 pp. [Available online at https://pubs.usgs.gov/pp/1286/report.pdf.]

Wright, D. B., J. A. Smith, and M. L. Baeck, 2014: Flood frequency analysis using radar rainfall fields and stochastic storm transposition. *Water Resour. Res.*, **50**, 1592–1615, doi:10.1002/2013WR014224.

Yue, S., 1999: Applying bivariate normal distribution to flood frequency analysis. *Water Int.*, **24**, 248–254, doi:10.1080/02508069908692168.

Zhu, L., S. M. Quiring, and K. A. Emanuel, 2013: Estimating tropical cyclone precipitation risk in Texas. *Geophys. Res. Lett.*, **40**, 6225–6230, doi:10.1002/2013GL058284.